Absence of CD14 delays progression of prion diseases accompanied by increased microglial activation

Running title: Prion infection in CD14-deficient mice

Keiko Sakai[a], Rie Hasebe[a], Yusuke Takahashi[a], Chang-Hyun Song[a,*], Akio Suzuki[a], Takeshi Yamasaki[a], Motohiro Horiuchi[a]

[a]Laboratory of Veterinary Hygiene, Graduate School of Veterinary Medicine, Hokkaido University, Nishi 9, Kita 18, Kita-ku, Sapporo 060-0818, Japan

Correspondence to Motohiro Horiuchi

E-mail: horiuchi@vetmed.hokudai.ac.jp; Tel & Fax: +81-11-706-5293

K. S. and R. H. contributed equally to this work.

*Present address

Department of Anatomy and Histology, College of Korean Medicine, Daegu Haany University, Gyeongsan, 712-715, Korea

Word counts: Abstract, 231; Text, 4954

Abstract

Prion diseases are fatal neurodegenerative disorders characterized by accumulation of PrP^{Sc}, vacuolation of neurons and neuropil, astrocytosis, and microglial activation. Up-regulation of gene expressions of innate immunity-related factors including complement factors and CD14 is observed in the brains of mice infected with prions even in the early stage of infections. When CD14 knockout ($CD14^{-/-}$) mice were infected intracerebrally with the Chandler and Obihiro prion strains, the mice survived longer than wild-type (WT) mice, suggesting that CD14 influences the progression of the prion disease. Immunofluorescence staining that can distinguish normal prion protein from the disease-specific form of prion protein (PrP^{Sc}) revealed that deposition of PrP^{Sc} was delayed in $CD14^{-/-}$ mice when compared with WT mice by the middle stage of the infection. Immunohistochemical staining with Iba1, a marker for activated microglia, showed an increased microglial activation in prion-infected $CD14^{-/-}$ mice than in WT mice. Interestingly, accompanied by the increased microglial activation, anti-inflammatory cytokines IL-10 and TGF-β, appeared to be expressed earlier in prion-infected $CD14^{-/-}$ mice. In contract, IL-1β expression appeared to be reduced in the $CD14^{-/-}$ mice in the early stage of infection. Double immunofluorescence staining demonstrated that CD11b- and Iba1-positive microglia mainly produced the anti-inflammatory cytokines, suggesting anti-inflammatory status of microglia in the $CD14^{-/-}$ mice in the early stage of infection. These results imply that CD14 plays a role in the disease progression by suppressing anti-inflammatory responses in the brain in the early stage of infection.

Introduction

Prion diseases are fatal neurodegenerative disorders including scrapie in sheep and goats, bovine spongiform encephalopathy in cattle, chronic wasting disease in cervids, and Creutzfeldt-Jakob disease in humans. These diseases are characterized by the deposition of disease specific prion protein (PrP^{Sc}), vacuolation of neurons and neuropil, and astrocytosis in the central nervous system (CNS). Despite little recruitment of adaptive immune cells into the CNS in prion diseases, microglial activation has been observed close to depositions of PrP^{Sc} before neuronal degeneration occurs (1, 2).

Microglia, the resident macrophages of the CNS, survey the environment in the physiological condition. Microbial infections, injury, and neurodegenerative conditions induce microglial activation characterized by changes in the shape, gene expression, and function including cytokine production, phagocytic activity, and antigen presentation (3, 4). Activated microglia are neurotoxic by producing pro-inflammatory mediators such as interleukin (IL)-1β, IL-6, tumor necrosis factor (TNF)-α, nitric oxide, and reactive oxygen species (5). Alternatively, activated microglia are neuroprotective by blocking pro-inflammatory responses and producing anti-inflammatory cytokines IL-10, transforming growth factor (TGF)-β and neurotrophic factors (6).

Previous studies have suggested the significance of a pro-inflammatory environment in the CNS in the progression of prion diseases. Schultz et al. demonstrated that IL-1β receptor I-deficient mice delayed the onset of prion diseases with attenuated PrP^{Sc} deposition and astrocytosis (7). A protective role of anti-inflammatory cytokines in prion diseases have also been reported: The incubation time in IL-10 deficient mice was greatly shortened (8). Boche et al. showed that inhibition of TGF-β activity in ME7 prion-infected mice induced severe

neuronal inflammation and acute neuronal death (9). Taken together these facts suggest the necessity of the inflammatory environment in the brains of prion-infected mice to be further elucidated for a better understanding of the mechanism of neurodegeneration in prion diseases.

It is well established that PrP^{Sc} accumulation precedes neurodegeneration and clinical manifestations of prion diseases. To analyze the host reaction in prion infection in the brain particularly during the early stages after intracerebral inoculation of prions, we compared the gene expression of prion- and mock-infected mouse brains by cDNA microarray analysis from 60 to 90 days post inoculation (dpi) (M.H. & C-H.S., unpublished observations). Focusing on genes which have been reported to be expressed by microglia, we found that several innate-immunity-related genes including *CD14* and complement factors were up-regulated as described in previous studies (10, 11) The CD14, a GPI-anchored protein, is well known as a lipopolysaccharide (LPS) receptor. Although CD14 itself cannot induce cellular signaling because of lack of cytoplasmic domains, binding of pathogen associated molecular patterns to CD14 clusters transmembrane proteins including Toll-like receptor (TLR) 2 and 4 to induce gene expression of pro-inflammatory mediators (12, 13). Up-regulation of CD14 expression associated with deposits of aggregated proteins has been reported in the brains of mouse models and human patients with neurodegenerative disorders including Alzheimer's disease (AD), Parkinson's disease/dementia with Lewy bodies, and amyotrophic lateral sclerosis (14). A polymorphism in the promoter region of the *CD14* gene that affects the expression of *CD14* has been reported to significantly increase the risk of Parkinson's disease in females (15, 16). Depletion of CD14 in an AD mouse model showed a reduced amyloid β (Aβ) plaque burden with altered microglial activation (17). These findings

suggest the involvement of CD14 in the pathogenesis of neurodegenerative disorders.

In the present study, we examined if CD14 influences the neuropathology and neuro-inflammatory conditions in prion diseases. When CD14 knockout ($CD14^{-/-}$) mice were inoculated intracerebrally with Chandler and Obihiro prion strains, the survival time was significantly prolonged when compared with wild type (WT) mice, suggesting that CD14 is involved in the progression of the disease. Our data also suggest that an increased microglial activation in $CD14^{-/-}$ mice accompanied by anti-inflammatory cytokine production may contribute to the prolonged survival time of the $CD14^{-/-}$ mice.

Materials and Methods

Antibodies. Anti-mouse prion protein (PrP) monoclonal antibodies (mAbs) 31C6 and 132 were prepared as described previously (18). Anti-Iba1 rabbit polyclonal antibodies were purchased from Wako (Product No. 019-20001). Anti-glial fibrillary acidic protein (GFAP) rabbit polyclonal antibodies were from Dako (Product No. Z033401). Un-conjugated and Alexa Fluor 488-conjugated anti-mouse CD11b rat mAb (clone M1/70, anti-mouse CD14 rat mAb (clone Sal 14-2) and anti-mouse F4/80 rat mAb (clone BM8) were from BioLegend. Anti-NeuN mouse mAb (clone A60) was from Millipore. Anti-mouse CD45 rat mAb (clone 13/2.3) was from Funakoshi. Anti-GFAP mouse mAb (clone GF5), anti-IL-10 rat mAb (clone JES5-2A5), anti-mouse CD68 rat mAb (clone FA-11), anti-TGF-β rabbit polyclonal antibodies (Product No. 66043) and anti-IL-1β rabbit polyclonal antibodies (Product No. 9722) were from Abcam. ECL Horse radish peroxidase-labeled anti-mouse IgG was from Amersham Biosciences (Product No. NA9310V). All Alexa Fluor-labeled antibodies were

from Life Technologies.

Mice and prion inocluation. C57BL/6J mice were purchased from Japan Clea Inc. CD14 knockout ($CD14^{-/-}$) mice congenic strain B6.129S-$Cd14^{<tm1Frm>}$/J were purchased from Jackson Laboratories and were further maintained by inbreeding. All animal procedures were approved by the Institutional Animal Care and Use Committee of the Graduate School of Veterinary Medicine, Hokkaido University. Six-week-old female WT and $CD14^{-/-}$ mice were inoculated intracerebrally with 20 μl of 2.5% brain homogenates of the Chandler- or Obihiro-infected C57BL/6J mice. The inoculation was carried out whenever the six-week-old female $CD14^{-/-}$ mice were available. The exact same aliquots of 2.5% brain homogenates were used for each inoculation. In the clinical stage, mice were observed everyday and the clinical endpoint of disease was defined as recumbency with severe emaciation within two consecutive days.

Quantitative RT-PCR. Total RNA was extracted from the thalamus cut at a thickness of the coronal section with 5 mm around the level of bregma -1.82 mm from "The Mouse Brain, 2nd edition" (19) using TRIZOL reagent (Life Technologies). First-strand cDNA was synthesized from 2 μg of the total RNA using a First-Strand cDNA synthesis kit (Amersham Biosciences) according to the manufacturer instructions. The amplification reaction mixtures contained template cDNA, 1× predesigned TaqMan Gene Expression Assays for mouse Cd14 (Mm00438094_g1) and for mouse ACTB (Code No. 432933E), and 1× TaqMan Fast Universal PCR Master Mix. TaqMan assays were carried out using an ABI 7900HT Fast Real-Time PCR system (Applied Biosystems). The amplification profiles were analyzed using

137 a threshold cycle relative quantification method and were normalized with the expression of
138 mouse ACTB gene as described previously (20).
139
140 ***Bioassay.*** Brain homogenates from 2 mice at each time point were prepared in sterile PBS to
141 1% (w/v). Twenty microlitters of brain homogenates were inoculated intracerebrally into
142 6-week-old Tga20 mice. To obtain an infectivity-incubation time standard curve, 10-fold
143 serial diluted brain homogenates used as the inocula of the Chandler and Obihiro strains were
144 also injected into Tga 20 mice. The 50% lethal dose (LD_{50}) of the original 10% homogenates
145 was estimated to be $10^{9.3}$ and $10^{9.5}$ LD_{50}/g brain tissue for the Chandler and Obihiro strains,
146 respectively. In the Chandler infection, the standard curve for the incubation periods (χ) was
147 fitted by the approximation of concentrations of original brain homogenates (y), $y = e^{23.026-0.425\chi}$
148 for the periods up to 68 days and $y = e^{16.118-0.332\chi}$ for the periods after 69 days. In
149 the Obihiro infection, the approximation was $y = e^{20.723-0.263\chi}$ for the periods up to107 days and
150 $y = e^{7.092-0.129\chi}$ for the periods after 108 days.
151
152 ***Protease-resistant prion protein (PrP-res) detection by immunoblotting.*** At 60, 90, 120 dpi,
153 and at the terminal stage of the disease, brains were harvested and were homogenized in
154 sterile phosphate-buffered saline (PBS) to prepare 10% (w/v) brain homogenates. The
155 homogenates were treated with proteinase K (PK) and were subjected to SDS-PAGE and
156 immunoblotting as described previously (20).
157
158 ***PrP^{Sc}-specific immunofluorescence staining.*** The PrP^{Sc}-specific staining of frozen sections
159 was performed by the method described previously (21) with some modifications. Briefly, the

brains were embedded in the OCT compound (Sakura Finetek, Japan) and were cut at the thickness of 10 μm. The samples were fixed with 4% paraformaldehyde (PFA) for 10 min at room temperature (rt). The slides were treated with 0.1% Triton X-100 for 10 min at rt, and then with 5M guanidine thiocyanate for 10 min at rt. After washing with PBS, the sections were blocked with 5% FBS in PBS at 37˚C for 30 min. The sections were then incubated with mAb132 at 3 μg/ml at 37˚C for 45 min. For the secondary antibody reaction, the sections were incubated with Alexa Fluor 488-labeled anti-mouse IgG (Fab)'$_2$ fragment of goat IgG at rt for 1 h. The samples were counterstained with 4'6-Diamidino-2-Phenylindole (DAPI), mounted with ProLong Gold anti-fade reagent (Invitrogen) and then observed with an LSM confocal microscope (Carl Zeiss International).

Histopathological analysis. The histopathological analysis was carried out as described previously (22). Briefly, brains were harvested at 90, 120 dpi and the terminal stage of the disease and fixed with 10% phosphate-buffered formalin. The brains were embedded in paraffin and cut at the level of bregma -1.82 mm. The samples were stained with Hematoxylin & Eosin (HE) staining.

Immunohistochemistry. For the antigen retrieval of Iba1 detection in paraffin embedded tissue, the slides were treated with microwaves at 600W for 10 min in 0.01M Citrate buffer solution pH6.0. After washing with PBS, the slides were blocked with normal goat serum (Nichirei) and incubated overnight with primary antibody diluted at 1:1000 in normal goat serum at 4˚C. The slides were treated with 0.3% hydrogen peroxide in methanol to block endogenous peroxidase activity at rt for 10 min. Biotin-labeled anti-rabbit IgG goat

polyclonal antibodies (Nichirei) were incubated for 10 min at rt. Peroxidase-labeled streptoavidin (Nichirei) was reacted for 5 min at rt. The immunoreactivity was visualized with Impact DAB (Vector). For the quantitative analysis of the number of Iba1-positive microglia, cells with more than 10 μm^2 of Iba1 immunoreactivity was counted by Image J (Rasband, W. S. Image J, U. S. National Institute of Health, Bethesda, Maryland, USA, http://rsb.info.nih.gov/ij/, 1997-2009).

For the immunohistochemistry of the microglial markers and cytokines in frozen tissue, brains were embedded in the OCT compound (Sakura Finetek Japan) and were cut at a thickness of 10 μm. Sections were fixed with 4% PFA for 10 min at rt. For the antigen retrieval, samples were treated with 0.1% Tween20 in PBS for 15 min at rt. The slides were blocked with 2% bovine serum albumin for 15 min at rt, incubated overnight with primary antibody at 4˚C. Then, slides were incubated with secondary antibodies and DAPI for 1h at rt. Finally slides were mounted with ProLong Gold Anti-fade Reagent (Invitrogen) and observed with LSM700 (Zeiss) or (Nikon). For the detection of CD14, CD45, and CD68, the antibodies were diluted at 1:800. For CD11b, TGF-β, and IL-1β, the antibodies were diluted at 1:200. For IL-10, the antibody was diluted at 1:100. For GFAP and F4/80, the antibodies were diluted at 1:1000. For secondary antibodies, all Alexa Fluor-labeled antibodies were diluted at 1:1000.

Results

Expression of CD14 is increased in microglia accompanied by progression of prion diseases. Previous DNA microarray analyses have suggested that gene expression of *CD14*

was up-regulated in prion-infected mouse brains in the early stage of infection (10, 11) (M.H. & C-H.S., unpublished observation). To confirm the gene expression of *CD14*, we performed a quantitative RT-PCR (Fig. 1A). The *CD14* gene expression in the thalamus of the Chandler-infected mice was 2.5 ± 0.8, 3.6 ± 0.8, and 3.6 ± 0.6 higher than that in the thalamus of mock-infected mice, at 75, 90, and 120 dpi, respectively, confirming the up-regulation of *CD14* expression. We also performed immunofluorescence staining of frozen sections of the Chandler- and Obihiro-infected mice brains to confirm the protein expression of CD14 (Fig. 1B), and CD14-positive cells were most frequently detected in the cerebral peduncle at the observed time points (Fig. 1B). The CD14-positive cells were scattered in corpus callosum, internal capsules, and cerebral peduncles at 60 dpi, spreading more widely in the cerebral peduncles and periventricle areas at 90 dpi, and the spreading had expanded to the thalamus at 120 dpi (Fig. 1B & C). A few CD14-positive cells were also detected in the internal capsules and cerebral peduncles of mock-infected mouse brains suggesting that these cells may be residents in these areas (Fig. 1C). To confirm the CD14 expression in the microglia, double staining of the CD14 with CD11b for microglia and of the GFAP for astrocytes were performed (Fig. 1D). Most of the CD14 immunoreactivity was detected in the CD11b-positive microglia, but it was not detected in the GFAP-positive astrocytes.

CD14 influences the progression of prion diseases. To examine the effect of the lack of CD14 on the neuropathogenesis of prion diseases, we inoculated brain homogenates of the Chandler or Obihiro strain-infected mice into $CD14^{-/-}$ mice (Fig. 2). The $CD14^{-/-}$ mice infected either with the Chandler or Obihiro strains survived longer than the WT mice. The mean survival time of the Chandler strain-infected $CD14^{-/-}$ mice (161.7 ± 3.7 days, n = 11)

was significantly longer than that of the WT mice (153.8 ± 3.7 days, n = 12, $p<0.01$, Student's *t*-test, Figs. 2A). The mean survival time of the Obihiro strain-infected $CD14^{-/-}$ mice (172.3 ± 4.8 days, n = 10) was also significantly longer than that of WT mice (157.9 ± 7.8 days, n = 11, $p<0.01$, Student's *t*-test, Fig. 2B). These results suggest that the lack of CD14 decelerates the progression of the disease.

To determine if knockout of CD14 influences the accumulation of PrP^{Sc}, we analyzed the PrP-res accumulation in the brains by immunoblotting (Figs. 3A & B). The intensity of the PrP^{Sc} signals in the brains of $CD14^{-/-}$ mice infected with either the Chandler or the Obihiro strains was slightly reduced at 90 and 120 dpi, and became comparable to those of the WT mice at the terminal stage.

We have reported that mAb132 recognizing amino acid 119-127 of mouse PrP, in combination with pre-treatment of cells with 5M guanidine thiocyanate, is useful for the PrP^{Sc}-specific immunofluorescence staining of prion-infected cell cultures (21). It is well established that PrP^{Sc} includes protease-sensitive and protease-resistant PrP^{Sc} (23, 24). The protease-sensitive PrP^{Sc} that cannot be detected by immunoblotting using proteinase K-treated samples could be detected by this PrP^{Sc}-specific immunofluorescence staining because of the omission of protease treatment process. In the present study we applied this method to brain frozen sections for the detection of PrP^{Sc} (Figs. 3C & D). Signals of PrP could be detected from the brains of prion-infected mice but signals from the brains of uninfected mice remained at background levels under the same condition (data not shown), demonstrating that this method can be applied to detect PrP^{Sc} from brain frozen sections. At 60 dpi, bright punctuate staining of PrP^{Sc} was detected frequently in the thalamus and occasionally detected in the cerebral cortex of the WT mice infected with the Chandler strain. The PrP^{Sc} was also

252 detected in parts of the thalamus of CD14$^{-/-}$ mice, but the occurrence was less frequent than in
253 the same areas of WT mice (Figs 3C & D). At 90 dpi, PrP^{Sc} was distributed more widely;
254 PrP^{Sc} could be detected in the hippocampus as well as in the thalamus and cerebral cortex of
255 WT and CD14$^{-/-}$ mice infected with the Chandler strain (Fig. 3D). However, the PrP^{Sc} staining
256 in some brain areas of CD14$^{-/-}$ mice seemed to be still weaker than in the WT mice (Figs. 3C
257 & D). There were no marked differences in the PrP^{Sc} distribution between the WT and CD14$^{-/-}$
258 mice at 120 dpi. Delay of the PrP^{Sc} accumulation was also observed in the brains of the
259 Obihiro-infected CD14$^{-/-}$ mice. At 60 dpi, PrP^{Sc} was detected in the hippocampus and
260 thalamus of WT mice, but not in these areas of the CD14$^{-/-}$ mice. At 90 dpi, PrP^{Sc} was spread
261 into the hypothalamus and amygdala of WT mice, but the presence of PrP^{Sc} in the CD14$^{-/-}$
262 mice was restricted to the hippocampus and thalamus.

263 We also analyzed the prion infectivity in the brains of WT and CD14$^{-/-}$ mice using Tga20
264 mice that overexpress mouse PrP and thus are highly susceptible to mouse-adapted prions
265 (25). Prion infectivity in the brains of both of 2 Chandler-infected CD14$^{-/-}$ mice at 60 dpi were
266 significantly lower than those from both of 2 WT mice (Fig. 4). Prion infectivity in the brains
267 of the Obihiro-infected mice also appeared to be lower than those from WT mice; the
268 infectivity in the brain of one CD14$^{-/-}$ mouse (No.2) was significantly lower than those of one
269 WT mouse (No.1). However, in the later stages, there were no significant differences in the
270 prion infectivity of WT and CD14$^{-/-}$ mice in the Chandler- or Obihiro-infection (Fig. 4)

271 We also performed a histopathological analysis of the brains of WT and CD14$^{-/-}$ mice
272 infected with the Chandler strain (Fig. 5). At 90 dpi, slight vacuolar degeneration of neuropil
273 and neurons was only occasionally observed in in the thalamus of Chandler-infected WT and
274 CD14$^{-/-}$ mice. Vacuolar degeneration was widely observed throughout the brains after 120 dpi;

however, there was no apparent difference in the severity and distribution of vacuolar degeneration of the WT and CD14$^{-/-}$ mice infected with the Chandler strain.

Microglial activation. Depletion of CD14 in a mouse model of Alzheimer's disease (AD) was reported to result in a reduction in the number of microglia (17). To assess if depletion of CD14 altered microglial activation in prion diseases, we analyzed the expression of an activated microglial marker Iba1 by immunohistochemistry (Fig. 6). At 60 dpi, some microglia of CD14$^{-/-}$ mice had more protrusions than those of WT mice. Morphological differences in Iba1-positive microglia became more prominent at 90 dpi; microglia in CD14$^{-/-}$ mice had a larger cytoplasm and more branched protrusions than those of WT mice. At 120 dpi, Iba1-positive microglia in WT mice had a smaller cytoplasm and fewer protrusions; however, microglia in CD14$^{-/-}$ mice still had relatively larger cytoplasm with many protrusions. In the terminal stage, there were no obvious differences in the morphology of microglia between WT and CD14$^{-/-}$ mice.

The quantitative analysis of Iba1 positive microglia showed that in the hippocampus and thalamus of the Chandler-infected WT and CD14$^{-/-}$ mice the numbers of microglia increased from 60 to 120 dpi, then showed no further change or slightly decreased (Fig. 6B). Similar changes were observed in the Obihiro-infected WT and CD14$^{-/-}$ mice. In the Chandler-infected mice, there was little difference in the numbers of Iba1-positive microglia between the WT and CD14$^{-/-}$ mice by 90 dpi. At 120 dpi, Iba1-positive microglia increased more in the thalamus of CD14$^{-/-}$ mice than in WT mice. In the terminal stage, numbers of the Iba1-positive microglia decreased both in WT and CD14$^{-/-}$ mice, although those in the thalamus of CD14$^{-/-}$ mice were still slightly larger than those of WT mice. In the

298 Obihiro-infected mice, there were no differences in the numbers of Iba1-positive microglia
299 between the WT and CD14$^{-/-}$ mice at 60 dpi. At 90 and 120 dpi, numbers of Iba1-positive
300 microglia in the thalamus of CD14$^{-/-}$ mice appeared to be larger than in the thalamus of WT
301 mice. In the terminal stage, there were no marked differences in the numbers of Iba1-positive
302 microglia between WT and CD14$^{-/-}$ mice.
303 To further characterize the differences in microglial activation of prion-infected WT and
304 CD14$^{-/-}$ mice, we performed immunofluorescence staining for other microglial markers (Fig.
305 7). Expression of CD11b, a commonly used microglial marker, was elevated in the brains of
306 WT and CD14$^{-/-}$ mice from 90 to 120 dpi, and the expression of CD11b in CD14$^{-/-}$ mice was
307 more intense than that in WT mice at each time point. A marker for macrophages and
308 monocytes, F4/80, is also frequently used as a microglial marker. Similar to CD11b, F4/80
309 immunoreactivity was detected more in CD14$^{-/-}$ mice than in WT mice at 90 and 120 dpi.
310 Similar changes were also observed in the immunofluorescence staining for CD68, a
311 phagocytic marker of macrophages and microglia: CD68-positive cells increased
312 time-dependently both in WT and CD14$^{-/-}$ mice, and CD68 immunoreactivity was more
313 prominent in CD14$^{-/-}$ mice than in WT mice. We also analyzed CD45, a common leukocyte
314 antigen expressed on all leukocytes. Ramified parenchymal microglia express lower levels of
315 CD45 than peripheral macrophages (26, 27) , while the expression of CD45 in microglia may
316 be increased in certain pathological conditions such as HIV encephalitis (28, 29) and
317 Alzheimer's disease (30). For the study here, expression of CD45 was clearly up-regulated
318 more in CD14$^{-/-}$ mice than in WT mice at 90 and 120 dpi (Fig. 7).
319
320 ***Expression of an anti-inflammatory cytokines.*** Depletion of CD14 in the AD model mouse

resulted in a reduced amyloid β (Aβ) plaque burden with the increased gene expression of anti-inflammatory cytokine, IL-10 (17). Similar to the reduced Aβ plaque burden in AD model mice lacking $CD14^{-/-}$, this study observed that accumulation of PrP^{Sc} in prion-infected $CD14^{-/-}$ mice was delayed by 90 dpi (Figs. 3C & D). The knockout of the *IL-10* gene has been shown to greatly shorten the survival time of prion-infected mice, suggesting a protective role of IL-10 in the progression of prion diseases (8). Therefore, we analyzed the anti-inflammatory cytokine expression in prion-infected $CD14^{-/-}$ mice to determine if a lack of CD14 modulates the inflammatory response in the brain.

Compared to the mock-infected mice, the prion-infected WT mice showed a weak but detectable IL-10 expression from 60 to 120 dpi. Interestingly, IL-10 immunoreactivity was observed more frequently in the thalamus of $CD14^{-/-}$ mice than in WT mice throughout the time of observation (Fig. 8A), and IL-10 immunoreactivity in $CD14^{-/-}$ mice appeared to increase from 60 to 90 dpi but to decrease from 90 to 120 dpi. The IL-10-positive areas were quantified and statistically analyzed if more than 3 mice were available. At 60 dpi, the areas positive for IL-10 in $CD14^{-/-}$ mice were significantly larger than WT mice (Fig. 8B, $p<0.01$, Student's *t*-test). The IL-10-positive areas in $CD14^{-/-}$ mice were also larger than those in WT mice at 90 and 120 dpi. We also examined the cell type in the brains expressing IL-10 by double staining (Figs. 8C-F). Most of the IL-10 immunoreactivity was detected in CD11b- or Iba1-positive microglia (Figs. 8C & D) and some in NeuN-positive neurons (Fig. 8E) both in the brains of WT and $CD14^{-/-}$ mice from 60 to 120 dpi. There was no IL-10 immunoreactivity detected in GFAP-positive astrocytes (Fig. 8F).We also analyzed another anti-inflammatory cytokine, TGF-β (Fig. 9A), which has been reported to play a role in the suppression of progression of prion diseases (9). At 60 dpi, TGF-β immunoreactivity was observed more

344 frequently in CD14$^{-/-}$ mice than WT mice infected with the Chandler or Obihiro strains.
345 Although no significant difference was observed in TGF-β-positive areas between WT and
346 CD14$^{-/-}$ mice at 60 dpi (p = 0.053, Student's *t*-test), the areas in two of three samples from the
347 CD14$^{-/-}$ mice was larger than in all samples from WT mice (Fig. 9B), suggesting this tendency.
348 However, little difference in the TGF-β immunoreactivitiy was observed between WT and
349 CD14$^{-/-}$ mice after 90 dpi (Figs. 9A & B). However, there was little difference in the TGF-β
350 imunoreactivitiy of WT and CD14$^{-/-}$ mice after 90 dpi. Double staining showed that TGF-β
351 immunoreactivity was detected mostly in CD11b- and Iba1-positive microglia (Figs. 9C & D),
352 and only occasionally in NeuN-positive neurons (Fig. 9E). Very little TGF-β
353 immunoreactivity was detected in GFAP-positive astrocytes (Fig. 9F).
354
355 ***Expression of pro-inflammatory cytokine.*** We also assessed if a lack of CD14 influenced the
356 expression of pro-inflammatory cytokines in the brains of prion-infected mice. Here we
357 focused on IL-1β, since a lack of IL-1β receptor signaling has been reported to delay the
358 progression of prion diseases (7). Different from the situation in anti-inflammatory cytokines,
359 more immunoreactivity of IL-1β was detected in WT mice than in CD14$^{-/-}$ mice at 60 and 90
360 dpi, particularly in the corpus callosum, internal capsules, and cerebral peduncles (Fig. 10A).
361 Quantitative analysis showed that IL-1β-positive areas in the internal capsule of WT mice was
362 significantly larger than those in the same areas of CD14$^{-/-}$ mice at 60 dpi (Fig. 10B, $p<0.05$,
363 Welch *t*-test). Also, IL-1β-positive areas of WT mice tended to be larger than those of CD14$^{-/-}$
364 mice at 90 and 120 dpi (Fig. 10B), although statistical analyses could not be carried out due to
365 the limited animal number (n = 2). The differences in the expression of IL-1β of WT and
366 CD14$^{-/-}$ mice appeared to be less prominent in the thalamus throughout the time of the

observations (data not shown).

Discussion

Prolonged survival of prion-infected CD14$^{-/-}$ mice and delayed PrP^{Sc} deposition in the brains suggest that CD14 plays a role in acceleration of disease progression after prion infection. Similarly, depletion of CD14 reduced Aβ deposition in a mouse model of AD (17), suggesting that CD14 could also play a role in other neurodegenerative disorders. However, microglial activation is different in prion-infected and AD model mice lacking CD14; microglia in CD14$^{-/-}$ mice infected with prions were more strongly activated than in WT mice particularly in the early stage of the disease, whereas there is reduced microglial activation in AD model mice lacking CD14 (17).

There is a line of evidence that microglial activation causes detrimental effects in prion diseases. For instance, there is a report that a blockade of the colony stimulating factor 1 receptor (CSF1R) signaling pathway reduced microglial proliferation in the brains of prion-infected mice and slowed the disease progression (31). Prion-infected mice deficient for CD40 ligand showed shortened incubation periods with increased microglial activation (32). Furthermore, prion-infected CXCR3 deficient mice survived longer than WT mice with reduced microglial activation, although prion propagation and PrP^{Sc} accumulation were accelerated (33). On the contrary, here we showed that microglia were more activated in prion-infected CD14$^{-/-}$ mice than in WT mice, but that prion-infected CD14$^{-/-}$ mice survived longer than WT mice. This result implies that microglial activation in the CD14$^{-/-}$ mice could offer a protective effect in the disease progression after prion infection. Particularly, the

390 relationship between the increased microglial activation and delayed PrP^{Sc} accumulation in
391 $CD14^{-/-}$ mice is intriguing. Priller et al. reported that during the course of prion infection,
392 resident microglia were firstly activated and thereafter bone-marrow derived microglia
393 colonized the brain of the prion-infected mice, and more than 50% of the microglia were
394 replaced by bone-marrow derived microglia by the onset of the disease (34). Thus it is
395 possible that the origin and activation state of microglia differ in the early and in the late
396 stages of prion diseases. Here we showed that the increased activation of microglia in
397 prion-infected $CD14^{-/-}$ is concomitant with the up-regulation of the anti-inflammatory
398 cytokine production such as IL-10 and the delayed PrP^{Sc} accumulation. The precise phenotype
399 of the microglia at this time point remains to be elucidated, but it is suggested that microglia
400 activated in the early stage of prion infection in the $CD14^{-/-}$ mice possess a neuroprotective
401 potential.

402 Although an accelerating role of CD14 in the progression of prion diseases is suggested
403 by the current study, the mechanism for how the CD14 works in the process of the disease
404 needs to be further elucidated. One possible involvement of CD14 indicated by the results of
405 the immunofluorescence staining for anti-inflammatory cytokines is that it down-regulates
406 alternative activation of microglia directly or indirectly. Induction of a pro-inflammatory
407 response is another possible function of CD14 in prion diseases. The CD14 is a
408 GPI-anchoring protein and thus lacks an intracellular domain, but it works together with the
409 TLR4 homodimer to induce cellular signaling involved in pro-inflammatory responses (12).
410 Therefore, a lack of CD14 affects the signaling through the CD14/TLR4 complex which
411 could be a cause of the longer survival of prion-infected $CD14^{-/-}$ mice. However, a previous
412 study showed that TLR4-signaling mutant mice, C3H/HeJ ($Tlr4^{Lps\text{-}d}$) mice, possessing a single

amino acid mutation in the cytopalmic domain were highly susceptible to prion infection, suggesting that TLR4 signaling can interfere with the disease progression (35). This is seemingly paradoxical to the results of our study here. However, TLR4 is not the only counterpart of CD14: CD14 is reported to form clusters with a TLR2-TLR6 heterodimer (36). Ablation of myeloid differentiation factor 88 (MyD88), an obligate signal transducer adaptor protein for TLRs, did not affect the neuropathology of prion diseases after intracerebral inoculation of prions, indicating that TLR-signaling through MyD88 resulting in NF-κb activation is not involved in prion neuropathognesis (37). However, as TLRs can utilize both MyD88-dependent and -independent pathways (38), TLR2 also utilizes the Toll/interleukin 1 receptor domain containing adaptor protein (39). Thus, it would seem possible that CD14 can transduce cellular signaling through an association with TLRs other than TLR4 and MyD88-independent pathways and be able to modulate the inflammatory milieu which may influence the pathogenesis of prion diseases.

In addition to reduced deposition of pathogenic agents, another similarity of $CD14^{-/-}$ mice in prion infection and the AD model is the up-regulation of the anti-inflammatory cytokine IL-10 (17). This makes it conceivable that the phenotype of the microglia shifted to an anti-inflammatory, alternative activation status, even though the TNF-α gene expression was also more up-regulated in the AD model mice with the $CD14^{-/-}$ background than in those with the WT background (17). Among anti-inflammatory cytokines, both IL-10 and TGF-β have been reported to be involved in the pathogenesis of prion diseases. Thackray et al. reported that survival times of IL-10 deficient mice was remarkably short (8), although the mouse genetic background greatly influences the effect of IL-10 on prion diseases (40), suggesting a significant suppressive role of this cytokine in the disease progression. Inhibition of TGF-β

activity facilitated cerebral inflammation and acute neuronal death in ME7-infected mice (9). IL-10 has been reported to have a neuroprotective role by blocking caspase-3-like activity (41). and TGF-β also promotes neuronal survival by up-regulating anti-apoptotic Bcl-2 family proteins (42). Therefore, an earlier expression of these anti-inflammatory cytokines may partially contribute to the prolonged survival of $CD14^{-/-}$ mice. Furthermore, both IL-10 and TGF-β provide anti-inflammatory effects by down-regulating pro-inflammatory mediators such as IL-1β, IL-6, and TNF-α, and NO (43-45). Indeed, expression of IL-1β in some brain regions of $CD14^{-/-}$ mice appeared to be lower than in WT mice (Fig. 10). However, it is also possible that the lower expression of IL-1β here resulted from a lack of TLR-CD14 signaling (46).

In AD model mice, bone-marrow derived microglia infiltrated from the peripheral circulation have protective potential against Aβ deposition and cognitive impairment in the early stage of the disease (47, 48), although it is controversial whether the protective effect is due to a clearance of Aβ by microglia (49, 50). However it is also possible that, later stage, increased Aβ production may overwhelm the microglial activity, or the pro-inflammatory milieu may decrease the phagocytic activity of microglia (51), or that microglia change the activation status to a more pro-inflammatory and neurotoxic phenotype (52). PrP^{Sc} is believed to be produced in intracellular organelles such as early and recycling endosomes as well as on the plasma membrane (53-55). This would seem to exclude microglia from any role in the clearance of PrP^{Sc} itself by phagocytosis in the early stage of infection, although microglia remove neurons damaged by PrP^{Sc} accumulation (1, 56). Thus, the delayed PrP^{Sc} accumulation in the early stage of the disease in $CD14^{-/-}$ mice may imply the existence of a brain niche with accelerated microglial activation that may provide anti-prion propagation

conditions particularly at the early stage of the disease.

In this study, we showed that the increased activation of microglia accompanied by the altered expression of anti-inflammatory cytokines is possibly involved in the prolonged survival times and delayed deposition of PrP^{Sc} in prion-infected $CD14^{-/-}$ mice. This suggests that a CD14-dependent signaling pathway in microglia plays some role in the acceleration of the disease progression. Further analyses of the activation states of microglia and microglial functions would provide a better understanding of the roles of microglia in prion pathogenesis.

Acknowledgements

This work was supported by a Grant-in-Aid for Science Research (A) (grant no. 23248050), a Grant for Challenging Exploratory Research (grant no. 23658233), a Grant-in-Aid for Young Researcher (B) (grant no. 23780303), a grant from the global COE program (F-001) and the Program of Founding Research Centers for Emerging and Reemerging Infectious Diseases, from the Ministry of Education, Culture, Sports, Science, and Technology, Japan. This work was also supported by grants for TSE research (H23-Shokuhin-Ippan-005), and Research on Measures for Intractable Diseases (grant no. H23-Nanchi-Ippan-013) from the Ministry of Health, Labour and Welfare of Japan. This work was also supported in a part by a Grant-in-Aid from the BSE Control Project of the Ministry of Agriculture, Forestry and Fisheries of Japan. We thank Zensho Co., Ltd, for the BSL3 facility.

References

1. **Williams A, Lucassen PJ, Ritchie D, Bruce M.** 1997. PrP deposition, microglial activation, and neuronal apoptosis in murine scrapie. Exp. Neurol. **144:**433-438.
2. **Giese A, Brown DR, Groschup MH, Feldmann C, Haist I, Kretzschmar HA.** 1998. Role of microglia in neuronal cell death in prion disease. Brain Pathol. **8:**449-457.
3. **Kettenmann H, Hanisch UK, Noda M, Verkhratsky A.** 2011. Physiology of microglia. Physiol. Rev. **91:**461-553.
4. **Ransohoff RM, Perry VH.** 2009. Microglial physiology: unique stimuli, specialized responses. Annu. Rev. Immunol. **27:**119-145.
5. **Block ML, Zecca L, Hong JS.** 2007. Microglia-mediated neurotoxicity: uncovering the molecular mechanisms. Nat. Rev. Neurosci. **8:**57-69.
6. **Neumann H, Kotter MR, Franklin RJ.** 2009. Debris clearance by microglia: an essential link between degeneration and regeneration. Brain **132:**288-295.
7. **Schultz J, Schwarz A, Neidhold S, Burwinkel M, Riemer C, Simon D, Kopf M, Otto M, Baier M.** 2004. Role of interleukin-1 in prion disease-associated astrocyte activation. Am. J. Pathol. **165:**671-678.
8. **Thackray AM, McKenzie AN, Klein MA, Lauder A, Bujdoso R.** 2004. Accelerated prion disease in the absence of interleukin-10. J. Virol. **78:**13697-13707.
9. **Boche D, Cunningham C, Docagne F, Scott H, Perry VH.** 2006. TGFbeta1 regulates the inflammatory response during chronic neurodegeneration. Neurobiol. Dis. **22:**638-650.
10. **Hwang D, Lee IY, Yoo H, Gehlenborg N, Cho JH, Petritis B, Baxter D, Pitstick R, Young R, Spicer D, Price ND, Hohmann JG, Dearmond SJ, Carlson GA, Hood LE.** 2009. A systems approach to prion disease. Mol. Syst. Biol. **5:**252.
11. **Xiang W, Windl O, Wunsch G, Dugas M, Kohlmann A, Dierkes N, Westner IM, Kretzschmar HA.** 2004. Identification of differentially expressed genes in scrapie-infected mouse brains by using global gene expression technology. J. Virol. **78:**11051-11060.
12. **Chow JC, Young DW, Golenbock DT, Christ WJ, Gusovsky F.** 1999. Toll-like receptor-4 mediates lipopolysaccharide-induced signal transduction. J. Biol. Chem. **274:**10689-10692.
13. **Kirschning CJ, Wesche H, Merrill Ayres T, Rothe M.** 1998. Human toll-like receptor 2 confers responsiveness to bacterial lipopolysaccharide. J. Exp. Med. **188:**2091-2097.
14. **Letiembre M, Liu Y, Walter S, Hao W, Pfander T, Wrede A, Schulz-Schaeffer W, Fassbender K.** 2009. Screening of innate immune receptors in neurodegenerative diseases: a similar pattern. Neurobiol. Aging **30:**759-768.
15. **Baldini M, Lohman IC, Halonen M, Erickson RP, Holt PG, Martinez FD.** 1999. A

Polymorphism* in the 5' flanking region of the CD14 gene is associated with circulating soluble CD14 levels and with total serum immunoglobulin E. Am. J. Respir. Cell Mol. Biol. **20:**976-983.

16. **Lin JJ, Chen CH, Yueh KC, Chang CY, Lin SZ.** 2006. A CD14 monocyte receptor polymorphism and genetic susceptibility to Parkinson's disease for females. Parkinsonism Relat. Disord. **12:**9-13.
17. **Reed-Geaghan EG, Reed QW, Cramer PE, Landreth GE.** 2010. Deletion of CD14 attenuates Alzheimer's disease pathology by influencing the brain's inflammatory milieu. J. Neurosci. **30:**15369-15373.
18. **Kim CL, Umetani A, Matsui T, Ishiguro N, Shinagawa M, Horiuchi M.** 2004. Antigenic characterization of an abnormal isoform of prion protein using a new diverse panel of monoclonal antibodies. Virology **320:**40-51.
19. **Paxinos G, Franklin KBJ.** 2001. The mouse brain in stereotaxic coordinates. Academic Press, San Diego ; Tokyo.
20. **Uryu M, Karino A, Kamihara Y, Horiuchi M.** 2007. Characterization of prion susceptibility in Neuro2a mouse neuroblastoma cell subclones. Microbiol. Immunol. **51:**661-669.
21. **Yamasaki T, Suzuki A, Shimizu T, Watarai M, Hasebe R, Horiuchi M.** 2012. Characterization of intracellular localization of PrP(Sc) in prion-infected cells using a mAb that recognizes the region consisting of aa 119-127 of mouse PrP. J. Gen. Virol. **93:**668-680.
22. **Song CH, Furuoka H, Kim CL, Ogino M, Suzuki A, Hasebe R, Horiuchi M.** 2008. Effect of intraventricular infusion of anti-prion protein monoclonal antibodies on disease progression in prion-infected mice. J. Gen. Virol. **89:**1533-1544.
23. **Pastrana MA, Sajnani G, Onisko B, Castilla J, Morales R, Soto C, Requena JR.** 2006. Isolation and characterization of a proteinase K-sensitive PrPSc fraction. Biochemistry **45:**15710-15717.
24. **Tzaban S, Friedlander G, Schonberger O, Horonchik L, Yedidia Y, Shaked G, Gabizon R, Taraboulos A.** 2002. Protease-sensitive scrapie prion protein in aggregates of heterogeneous sizes. Biochemistry **41:**12868-12875.
25. **Fischer M, Rulicke T, Raeber A, Sailer A, Moser M, Oesch B, Brandner S, Aguzzi A, Weissmann C.** 1996. Prion protein (PrP) with amino-proximal deletions restoring susceptibility of PrP knockout mice to scrapie. EMBO J. **15:**1255-1264.
26. **Ford AL, Goodsall AL, Hickey WF, Sedgwick JD.** 1995. Normal adult ramified microglia separated from other central nervous system macrophages by flow cytometric sorting. Phenotypic differences defined and direct ex vivo antigen presentation to myelin basic protein-reactive CD4+ T cells compared. J. Immunol. **154:**4309-4321.
27. **Becher B, Antel JP.** 1996. Comparison of phenotypic and functional properties of immediately ex vivo and cultured human adult microglia. Glia **18:**1-10.

28. **Cosenza MA, Zhao ML, Si Q, Lee SC.** 2002. Human brain parenchymal microglia express CD14 and CD45 and are productively infected by HIV-1 in HIV-1 encephalitis. Brain Pathol. **12:**442-455.
29. **Cosenza-Nashat MA, Kim MO, Zhao ML, Suh HS, Lee SC.** 2006. CD45 isoform expression in microglia and inflammatory cells in HIV-1 encephalitis. Brain Pathol. **16:**256-265.
30. **Masliah E, Mallory M, Hansen L, Alford M, Albright T, Terry R, Shapiro P, Sundsmo M, Saitoh T.** 1991. Immunoreactivity of CD45, a protein phosphotyrosine phosphatase, in Alzheimer's disease. Acta Neuropathol. **83:**12-20.
31. **Gomez-Nicola D, Fransen NL, Suzzi S, Perry VH.** 2013. Regulation of microglial proliferation during chronic neurodegeneration. J. Neurosci. **33:**2481-2493.
32. **Burwinkel M, Schwarz A, Riemer C, Schultz J, van Landeghem F, Baier M.** 2004. Rapid disease development in scrapie-infected mice deficient for CD40 ligand. EMBO Rep **5:**527-531.
33. **Riemer C, Schultz J, Burwinkel M, Schwarz A, Mok SW, Gultner S, Bamme T, Norley S, van Landeghem F, Lu B, Gerard C, Baier M.** 2008. Accelerated prion replication in, but prolonged survival times of, prion-infected CXCR3-/- mice. J. Virol. **82:**12464-12471.
34. **Priller J, Prinz M, Heikenwalder M, Zeller N, Schwarz P, Heppner FL, Aguzzi A.** 2006. Early and rapid engraftment of bone marrow-derived microglia in scrapie. J. Neurosci. **26:**11753-11762.
35. **Spinner DS, Cho IS, Park SY, Kim JI, Meeker HC, Ye X, Lafauci G, Kerr DJ, Flory MJ, Kim BS, Kascsak RB, Wisniewski T, Levis WR, Schuller-Levis GB, Carp RI, Park E, Kascsak RJ.** 2008. Accelerated prion disease pathogenesis in Toll-like receptor 4 signaling-mutant mice. J. Virol. **82:**10701-10708.
36. **Henneke P, Takeuchi O, van Strijp JA, Guttormsen HK, Smith JA, Schromm AB, Espevik TA, Akira S, Nizet V, Kasper DL, Golenbock DT.** 2001. Novel engagement of CD14 and multiple toll-like receptors by group B streptococci. J. Immunol. **167:**7069-7076.
37. **Prinz M, Heikenwalder M, Schwarz P, Takeda K, Akira S, Aguzzi A.** 2003. Prion pathogenesis in the absence of Toll-like receptor signalling. EMBO Rep **4:**195-199.
38. **Kawai T, Akira S.** 2010. The role of pattern-recognition receptors in innate immunity: update on Toll-like receptors. Nat. Immunol. **11:**373-384.
39. **Kenny EF, Talbot S, Gong M, Golenbock DT, Bryant CE, O'Neill LA.** 2009. MyD88 adaptor-like is not essential for TLR2 signaling and inhibits signaling by TLR3. J. Immunol. **183:**3642-3651.
40. **Tamguney G, Giles K, Glidden DV, Lessard P, Wille H, Tremblay P, Groth DF, Yehiely F, Korth C, Moore RC, Tatzelt J, Rubinstein E, Boucheix C, Yang X, Stanley P, Lisanti MP, Dwek RA, Rudd PM, Moskovitz J, Epstein CJ, Cruz TD, Kuziel WA, Maeda N, Sap J, Ashe KH, Carlson GA, Tesseur I, Wyss-Coray T,**

Mucke L, Weisgraber KH, Mahley RW, Cohen FE, Prusiner SB. 2008. Genes contributing to prion pathogenesis. J. Gen. Virol. **89:**1777-1788.

41. **Bachis A, Colangelo AM, Vicini S, Doe PP, De Bernardi MA, Brooker G, Mocchetti I.** 2001. Interleukin-10 prevents glutamate-mediated cerebellar granule cell death by blocking caspase-3-like activity. J. Neurosci. **21:**3104-3112.
42. **Kim ES, Kim RS, Ren RF, Hawver DB, Flanders KC.** 1998. Transforming growth factor-beta inhibits apoptosis induced by beta-amyloid peptide fragment 25-35 in cultured neuronal cells. Brain Res. Mol. Brain Res. **62:**122-130.
43. **Bogdan C, Nathan C.** 1993. Modulation of macrophage function by transforming growth factor beta, interleukin-4, and interleukin-10. Ann. N. Y. Acad. Sci. **685:**713-739.
44. **Ledeboer A, Breve JJ, Poole S, Tilders FJ, Van Dam AM.** 2000. Interleukin-10, interleukin-4, and transforming growth factor-beta differentially regulate lipopolysaccharide-induced production of pro-inflammatory cytokines and nitric oxide in co-cultures of rat astroglial and microglial cells. Glia **30:**134-142.
45. **Seyler I, Appel M, Devissaguet JP, Legrand P, Barratt G.** 1997. Modulation of nitric oxide production in RAW 264.7 cells by transforming growth factor-beta and interleukin-10: differential effects on free and encapsulated immunomodulator. J. Leukoc. Biol. **62:**374-380.
46. **Fitzgerald KA, Rowe DC, Golenbock DT.** 2004. Endotoxin recognition and signal transduction by the TLR4/MD2-complex. Microbes and infection / Institut Pasteur **6:**1361-1367.
47. **El Khoury J, Toft M, Hickman SE, Means TK, Terada K, Geula C, Luster AD.** 2007. Ccr2 deficiency impairs microglial accumulation and accelerates progression of Alzheimer-like disease. Nat. Med. **13:**432-438.
48. **Simard AR, Soulet D, Gowing G, Julien JP, Rivest S.** 2006. Bone marrow-derived microglia play a critical role in restricting senile plaque formation in Alzheimer's disease. Neuron **49:**489-502.
49. **Grathwohl SA, Kalin RE, Bolmont T, Prokop S, Winkelmann G, Kaeser SA, Odenthal J, Radde R, Eldh T, Gandy S, Aguzzi A, Staufenbiel M, Mathews PM, Wolburg H, Heppner FL, Jucker M.** 2009. Formation and maintenance of Alzheimer's disease beta-amyloid plaques in the absence of microglia. Nat. Neurosci. **12:**1361-1363.
50. **Mildner A, Schlevogt B, Kierdorf K, Bottcher C, Erny D, Kummer MP, Quinn M, Bruck W, Bechmann I, Heneka MT, Priller J, Prinz M.** 2011. Distinct and non-redundant roles of microglia and myeloid subsets in mouse models of Alzheimer's disease. J. Neurosci. **31:**11159-11171.
51. **Koenigsknecht-Talboo J, Landreth GE.** 2005. Microglial phagocytosis induced by fibrillar beta-amyloid and IgGs are differentially regulated by proinflammatory cytokines. J. Neurosci. **25:**8240-8249.

52. **Jimenez S, Baglietto-Vargas D, Caballero C, Moreno-Gonzalez I, Torres M, Sanchez-Varo R, Ruano D, Vizuete M, Gutierrez A, Vitorica J.** 2008. Inflammatory response in the hippocampus of PS1M146L/APP751SL mouse model of Alzheimer's disease: age-dependent switch in the microglial phenotype from alternative to classic. J. Neurosci. **28:**11650-11661.

53. **Godsave SF, Wille H, Pierson J, Prusiner SB, Peters PJ.** 2013. Plasma membrane invaginations containing clusters of full-length PrP(Sc) are an early form of prion-associated neuropathology in vivo. Neurobiol. Aging **34:**1621-1631.

54. **Godsave SF, Wille H, Kujala P, Latawiec D, DeArmond SJ, Serban A, Prusiner SB, Peters PJ.** 2008. Cryo-immunogold electron microscopy for prions: toward identification of a conversion site. J. Neurosci. **28:**12489-12499.

55. **Jeffrey M, Goodsir CM, Bruce ME, McBride PA, Scott JR, Halliday WG.** 1992. Infection specific prion protein (PrP) accumulates on neuronal plasmalemma in scrapie infected mice. Neurosci. Lett. **147:**106-109.

56. **Hughes MM, Field RH, Perry VH, Murray CL, Cunningham C.** 2010. Microglia in the degenerating brain are capable of phagocytosis of beads and of apoptotic cells, but do not efficiently remove PrPSc, even upon LPS stimulation. Glia **58:**2017-2030.

661 **Figure legends**

662

663 Fig. 1. Expression of CD14 in the brains of prion-infected WT mice. (A) Gene expression of
664 *CD14*. Total RNA was extracted from the thalamus of Chandler- and mock-infected WT mice
665 at 75, 90, and 120 dpi and subjected to quantitative RT-PCR. Expression of the *CD14* gene in
666 the thalamus of the mock-infected mice at 75 dpi was defined as 1, and relative expressions
667 are shown. * $p<0.05$, ** $p<0.01$ (Student's *t*-test). (B) Immunofluorescence staining of CD14
668 in the cerebral peduncle. The brains of Chandler-, Obihiro-, and mock-infected mice were
669 harvested at 60, 90, and 120 dpi. Frozen sections at the level of bregma -1.82 mm were
670 subjected to immunofluorescence staining of CD14 (red). Blue, nuclear counterstaining with
671 DAPI. Bars show 50 μm. (C) Summary of the distribution of CD14 in the brains of Chandler-,
672 Obihiro-, and mock-infected mice. Illustrations show the level of bregma -1.82 mm from
673 "The Mouse Brain, 2nd edition" (19). (D) Double immunofluorescence staining of CD14
674 (green) with CD11b (left, red) or GFAP (right, red). Representative figures from the cerebral
675 peduncles of the Chandler-infected mice at 120 dpi are shown. Blue, nuclei. Bars show 20
676 μm.

677

678 Fig. 2. Survival times of WT and $CD14^{-/-}$ mice infected with the Chandler or Obihiro strains.
679 (A) Survival curves of the Chandler-infected WT and $CD14^{-/-}$ mice. (B) Survival curves of the
680 Obihiro-infected WT and $CD14^{-/-}$ mice.

681

682 Fig. 3. PrP^{Sc} accumulation in the brains of prion-infected WT and $CD14^{-/-}$ mice. (A) Detection
683 of PrP^{Sc} by immunoblotting. Brains were harvested at 90, 120 dpi, and the terminal stage.

Brain tissue equivalent loaded were 500, 350, and 250 μg for the 90, 120 dpi, and the terminal stage of the disease (term), respectively. Two mice were used in each group. M, Mw marker. (B) Quantitative analysis of the PrP^{Sc}. The results of immunoblotting were quantified using Multi Gauge ver 3.0 (Fuji Film). Each blot used 10 ng of rMoPrP for the normalization of the transfer efficiency and the graphs show relative values (arbitrary units, AU) to rMoPrP (average of the results from 2 mice). (C) Immunofluorescence staining of PrP^{Sc}. Frozen sections were prepared from the brains of WT and $CD14^{-/-}$ mice harvested at 60, 90, and 120 dpi and subjected to PrP^{Sc} specific staining with mAb 132. Representative images from the thalamus are shown (the regions of the boxed areas in the corresponding figures in Fig. 3D). Bars show 50μm. Green, PrP^{Sc}. Blue, nuclei. (D) Summary of PrP^{Sc} distribution detected by PrP^{Sc}-specific staining.

Fig. 4. Prion infectivity. (A, B) Prion infectivity in the brains of the Chandler (A) and Obihiro (B) strain infected WT and $CD14^{-/-}$ mice. The infectivity was measured by bioassay using Tga 20 mice. * $p<0.05$, ** $p<0.001$ by ANOVA followed Dunnett *host hoc* test. (C, D) Survival time of Tga 20 mice used for bioassay. Survival times of each Tga 20 mouse inoculated with brain homogenates from the Chandler-infected (C) and Obihiro-infected WT or $CD14^{-/-}$ mice (D) are shown. The difference in the Chandler-infected $CD14^{-/-}$ mice at 90 dpi was due to the small standard deviation of mouse No.1: three of four Tga20 mice in this group reached the terminal stage on the same day.

Fig. 5. Histopathological analysis of the brains of prion-infected WT and $CD14^{-/-}$ mice. Representative images from the thalamus, the hippocampus, and the cerebral peduncle of the Chandler-infected mice are shown. Bar: 50 μm.

Fig. 6. Expression of an activated microglial marker Iba1 in the brains of prion-infected WT and CD14$^{-/-}$ mice. (A) Immunohistochemistry for Iba1. Representative figures from the thalamus of the Chandler-infected mice are shown. Higher magnifications of the areas indicated by boxes are shown in the corresponding right panels. Bars show 20 μm. Term: Terminal stage. (B) Quantitative analysis of Iba1-positive microglia. Numbers of Iba1-positive cells in the hippocampus and the thalamus (1.5×10^{-1} mm^2 tissue section) were counted by Image J. Data of 2 mice from each group. T, Terminal stage; Hp, Hippocampus; Th, Thalamus.

Fig. 7. Immunofluorescence staining for microglial markers in the brains of prion-infected WT and CD14$^{-/-}$ mice. Frozen blocks of the brains harvested at 90 and 120 dpi were subjected to immunofluorescence staining for microglial markers CD11b, F4/80, CD68, and CD45. Representative images from the thalamus of the Chandler-infected mice are shown. Bars: 50 μm.

Fig. 8. Expression of IL-10 in the brains of WT and CD14$^{-/-}$ mice infected with the Chandler and Obihiro strains. (A) Immunofluorescence staining of IL-10. Frozen blocks of the brains harvested at 60, 90, and 120 dpi were subjected to Immunofluorescence staining. Representative figures from the thalamus at each time point are shown. Bars show 50 μm. Red, IL-10; Blue, nuclei. (B) Quantitative analysis of IL-10-positive areas in the thalamus of Chandler-infected mice. The areas positive for IL-10 (μm^2/0.1 mm^2) were quantified using Imaris ver 7.6.1 (Bitplane). The numbers of mice used for the analysis were 3 both of WT and

730 CD14$^{-/-}$ mice at 60 dpi, 2 both of WT and CD 14$^{-/-}$ mice at 90 dpi and 2 of WT mice at 120 dpi,
731 and 1 of CD14$^{-/-}$ mouse at 120 dpi. *p<0.01, Student's t-test. (C) – (F) Double
732 immunofluorescence staining of IL-10 with CD11b (C), Iba1 (D), NeuN (E), and GFAP (F).
733 Representative figures from the thalamus of the Chandler-infected mice are shown. Green
734 indicates immunoreactivities for these markers. Red, IL-10; Blue, nuclei. Arrows show double
735 positive cells. Bars: 10 μm.
736
737 Fig. 9. Expression of TGF-β in the brains of WT and CD14$^{-/-}$ mice infected with the Chandler
738 and Obihiro strains. (A) immunofluorescence staining of TGF-β at 60, 90, and 120 dpi.
739 Representative figures from the thalamus are shown for each time point. Bars show 50 μm.
740 Red, TGF-β; Blue, nuclei. (B) Quantitative analysis of TGF-β-positive areas in the thalamus
741 of Chandler-infected mice. The method and mice used for the quantification are the same as in
742 the legend for Fig. 8. (C) – (F) Double immunofluorescence staining of TGF-β with CD11b
743 (C), Iba1 (D), NeuN (E), and GFAP (F). Representative figures from the thalamus of the
744 Chandler-infected mice are shown. Green indicates immunoreactivities for these markers. Red,
745 TGF-β; Blue, nuclei. Arrows show double positive cells. Bars: 10 μm.
746
747 Fig. 10. Expression of IL-1β in the brains of prion-infected WT and CD14$^{-/-}$ mice. (A) (A)
748 Immunofluorescence staining of IL-1β in the internal capsule of mice infected with Chandler
749 or Obihiro strains at 60, 90 and 120 dpi. Bars show 50 μm. Red, IL-1β. Blue, nuclei. (B)
750 Quantitative analysis of IL-1β-positive areas in the thalamus of Chandler-infected mice. The
751 method and mice used for the quantification are the same as in the legend for Fig. 8. * p<0.01,
752 Welch t-test.
753

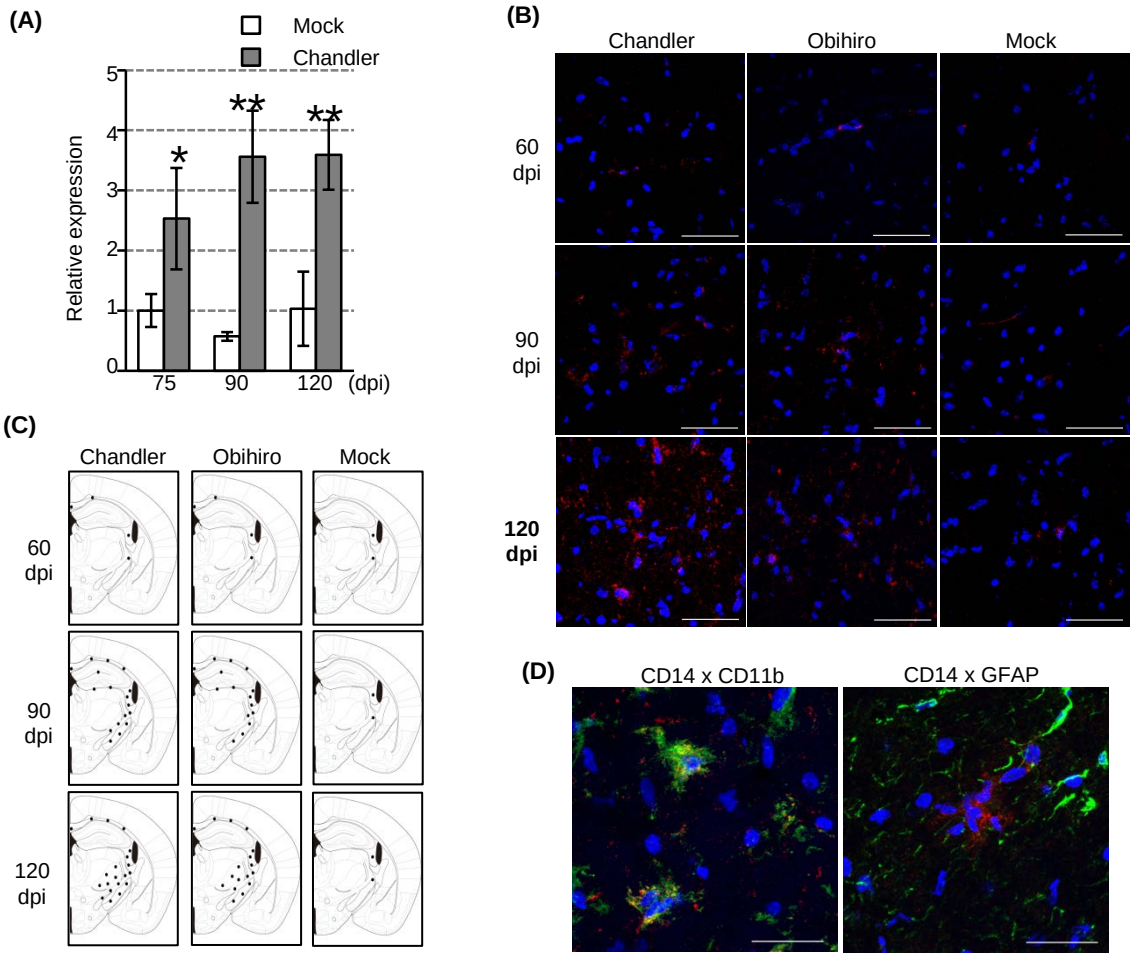

Fig. 1. Expression of CD14 in the brains of prion-infected WT mice. (A) Gene expression of *CD14*. Total RNA was extracted from the thalamus of Chandler- and mock-infected WT mice at 75, 90, and 120 dpi and subjected to quantitative RT-PCR. Expression of the *CD14* gene in the thalamus of the mock-infected mice at 75 dpi was defined as 1, and relative expressions are shown. * $p<0.05$, ** $p<0.01$ (Student's *t*-test). (B) Immunofluorescence staining of CD14 in the cerebral peduncle. The brains of Chandler-, Obihiro-, and mock-infected mice were harvested at 60, 90, and 120 dpi. Frozen sections at the level of bregma -1.82 mm were subjected to immunofluorescence staining of CD14 (red). Blue, nuclear counterstaining with DAPI. Bars show 50 μm. (C) Summary of the distribution of CD14 in the brains of Chandler-, Obihiro-, and mock-infected mice. Illustrations show the level of bregma -1.82 mm from "The Mouse Brain, 2nd edition" . (D) Double immunofluorescence staining of CD14 (green) with CD11b (left, red) or GFAP (right, red). Representative figures from the cerebral peduncles of the Chandler-infected mice at 120 dpi are shown. Blue, nuclei. Bars show 20 μm.

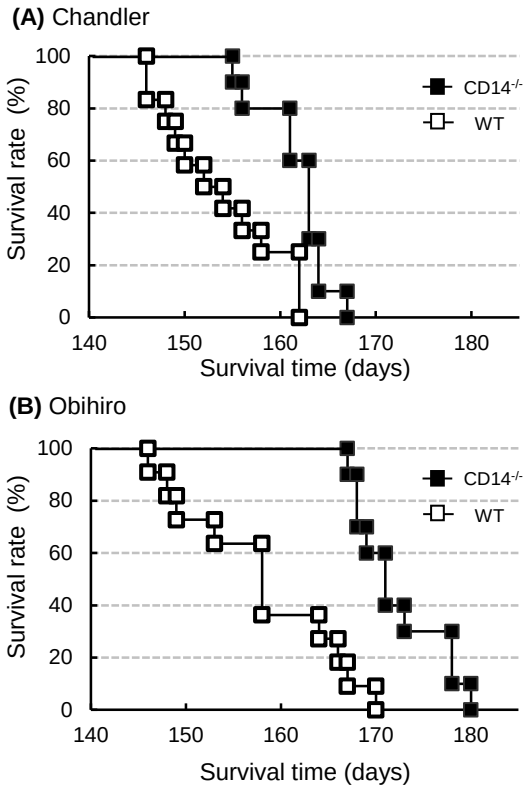

Fig. 2. Survival times of WT and CD14$^{-/-}$ mice infected with the Chandler or Obihiro strains. (A) Survival curves of the Chandler-infected WT and CD14$^{-/-}$ mice. (B) Survival curves of the Obihiro-infected WT and CD14$^{-/-}$ mice.

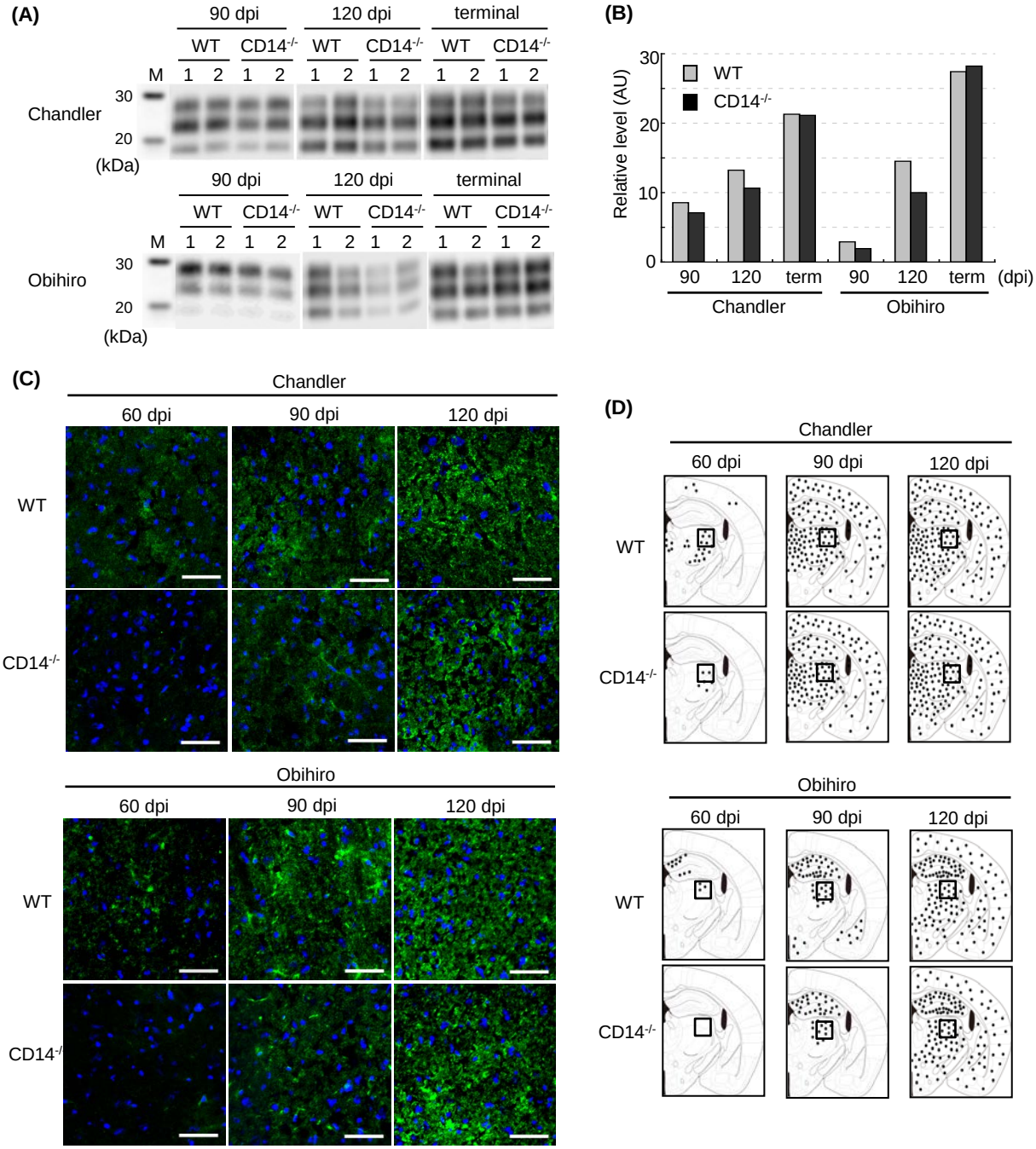

Fig. 3. PrP^{Sc} accumulation in the brains of prion-infected WT and $CD14^{-/-}$ mice. (A) Detection of PrP^{Sc} by immunoblotting. Brains were harvested at 90, 120 dpi, and the terminal stage. Brain tissue equivalent loaded were 500, 350, and 250 μg for the 90, 120 dpi, and the terminal stage of the disease (term), respectively. Two mice were used in each group. M, Mw marker. (B) Quantitative analysis of the PrP^{Sc}. The results of immunoblotting were quantified using Multi Gauge ver 3.0 (Fuji Film). Each blot used 10 ng of rMoPrP for the normalization of the transfer efficiency and the graphs show relative values (arbitrary units, AU) to rMoPrP (average of the results from 2 mice). (C) Immunofluorescence staining of PrP^{Sc}. Frozen sections were prepared from the brains of WT and $CD14^{-/-}$ mice harvested at 60, 90, and 120 dpi and subjected to PrP^{Sc} specific staining with mAb 132. Representative images from the thalamus are shown (the regions of the boxed areas in the corresponding figures in Fig. 3D). Bars show 50μm. Green, PrP^{Sc}. Blue, nuclei. (D) Summary of PrP^{Sc} distribution detected by PrP^{Sc}-specific staining.

(A) Chandler

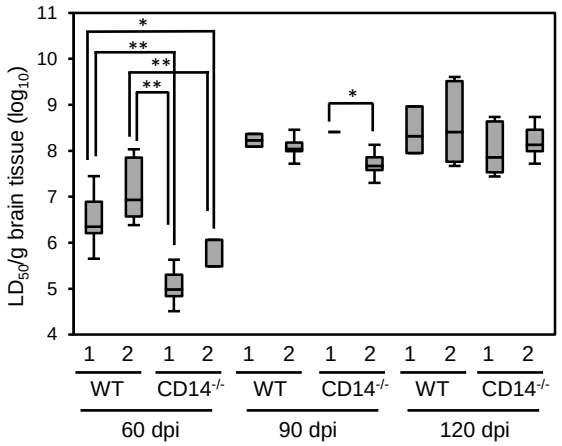

(C) Chandler

Inoculum	Mouse No.	Survival time (days)	Mean ± SD (days)
WT ,	1	65, 68, 69, 70, 72	68.7± 2.6
60 dpi	2	63, 64, 64, 67, 67, 70, 70	66.4 ± 2.9
CD14$^{-/-}$,	1	75, 78, 79, 81	78.3 ± 2.5
60 dpi	2	71, 71, 75, 75, 75	73.4 ± 2.2
WT,	1	60, 60, 60, 63	60.8 ± 1.5
90 dpi	2	59, 61, 61, 62	60.8 ± 1.3
CD14$^{-/-}$,	1	59, 59, 59, 60	59.2 ± 0.4
90 dpi	2	61, 63, 63, 65	63.0 ± 1.6
WT,	1	58, 58, 61, 63	60.0 ± 2.4
120 dpi	2	56, 56, 57, 59, 60, 65, 68	59.3 ± 4.5
CD14$^{-/-}$,	1	59, 59, 61, 63, 64, 66	62.0 ± 2.8
120 dpi	2	58, 60, 61, 62	60.2 ± 1.7

(B) Obihiro

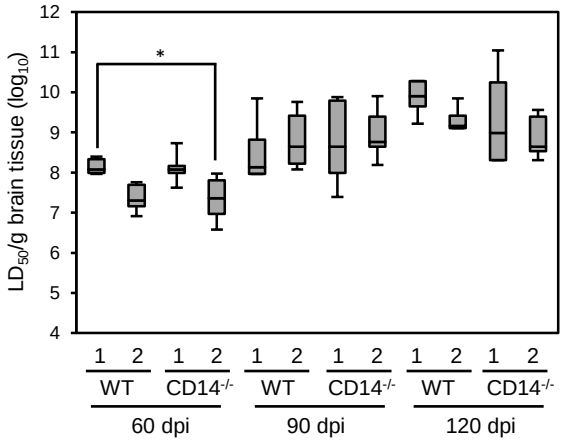

(D) Obihiro

Inoculum	Mouse No.	Survival time (days)	Mean ± SD (days)
WT ,	1	98, 98, 100, 100, 101, 101	99.7 ± 1.4
60 dpi	2	88, 104, 111, 113, 115, 119	108.3 ± 11.1
CD14$^{-/-}$,	1	95, 100, 100, 100, 101, 104	100.0 ± 2.9
60 dpi	2	107, 109, 111, 111, 111, 125, 125	114.1 ± 8.1
WT,	1	86, 89, 101, 101	96.5 ± 7.1
90 dpi	2	89, 91, 95, 95, 100, 100	95.0 ± 4.5
CD14$^{-/-}$,	1	90, 91, 99, 106	96.5 ± 7.5
90 dpi	2	85, 88, 91, 94, 94, 96	92.4 ± 4.8
WT,	1	83, 83, 85, 90	85.3 ± 3.3
120 dpi	2	85, 90, 91, 91	89.3 ± 2.8
CD14$^{-/-}$,	1	80, 87, 92, 98, 98	91.0 ± 7.7
120 dpi	2	88, 90, 95, 96, 98	93.4 ± 4.2

Fig. 4. Prion infectivity in the brains of (A) Chandler and (B) Obihiro infected WT and CD14$^{-/-}$ mice. The infectivity was measured by titration using Tga 20 mice. *p<0.05, **p<0.001 by ANOVA followed Dunnett *host hoc* test. (C) & (D) Survival time of Tga 20 mice inoculated with the brain homogenates of Chandler (C)- and Obihiro(D)-infected WT and CD14$^{-/-}$ mice.

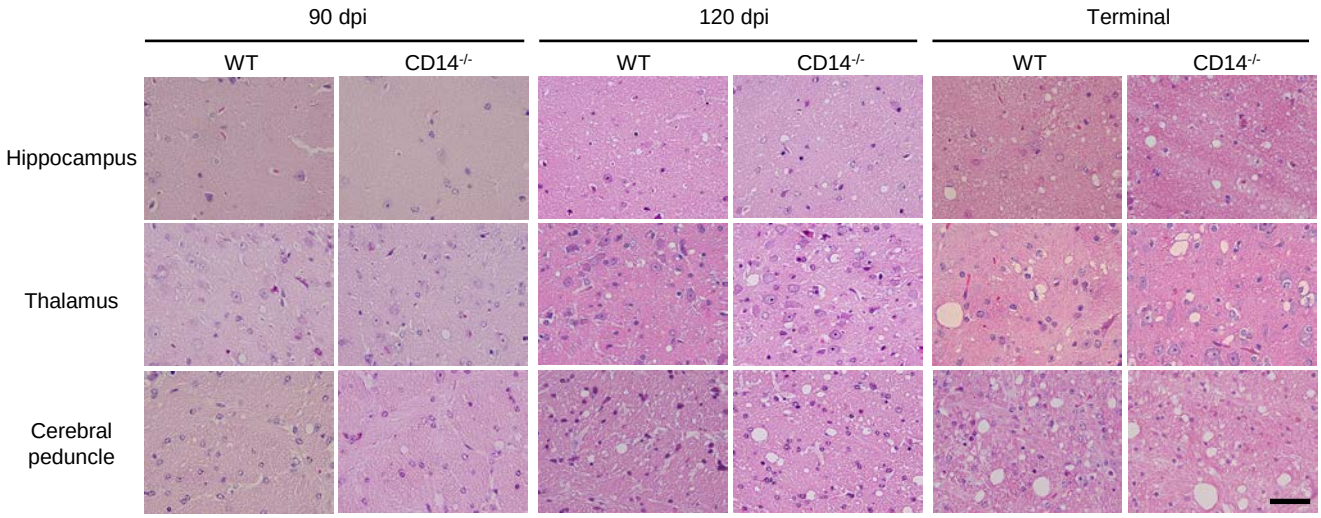

Fig. 5. Histopathological analysis of the brains of prion-infected WT and CD14$^{-/-}$ mice. Representative images from the thalamus, hippocampus, and cerebral peduncle of Chandler-infected mice are shown. Bar show 50 μm.

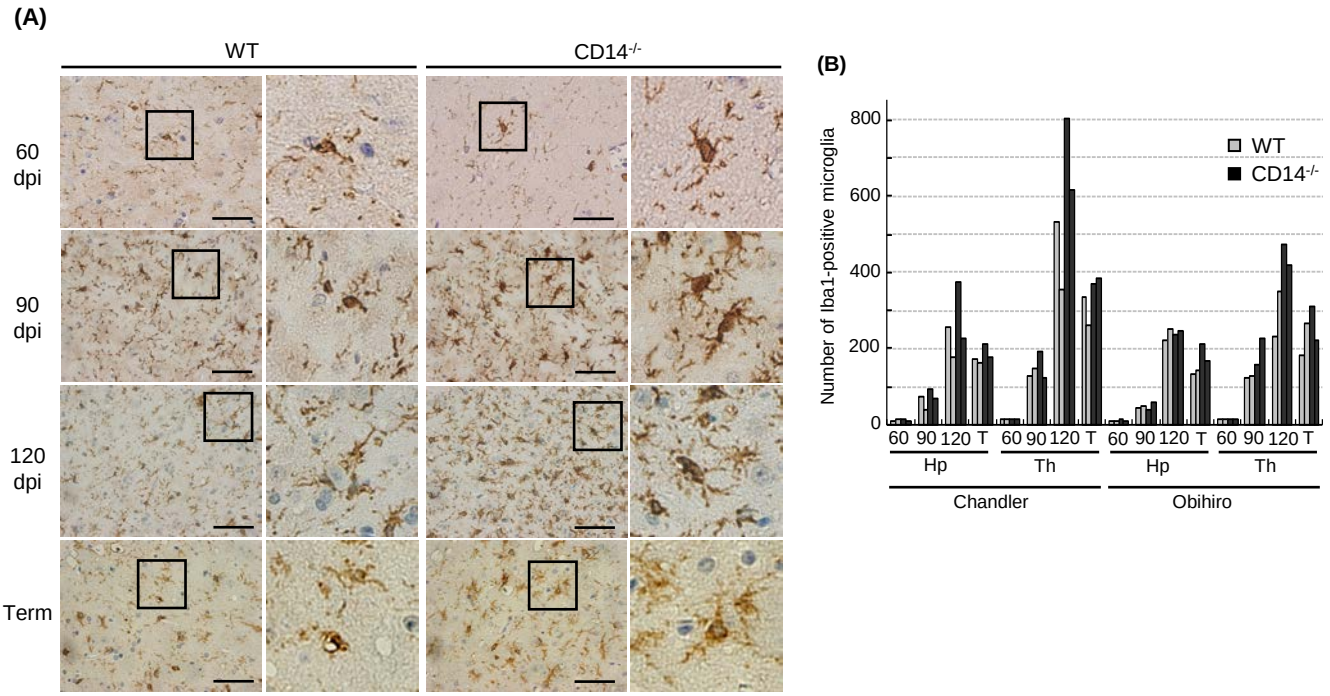

Fig. 6. Expression of an activated microglial marker Iba1 in the brains of prion-infected WT and CD14$^{-/-}$ mice. (A) Immunohistochemistry for Iba1. Representative figures from the thalamus of the Chandler-infected mice are shown. Higher magnifications of the areas indicated by boxes are shown in the corresponding right panels. Bars show 20 μm. Term: Terminal stage. (B) Quantitative analysis of Iba1-positive microglia. Numbers of Iba1-positive cells in the hippocampus and the thalamus (1.5×10^{-1} mm^2 tissue section) were counted by Image J. Data of 2 mice from each group. T, Terminal stage; Hp, Hippocampus; Th, Thalamus.

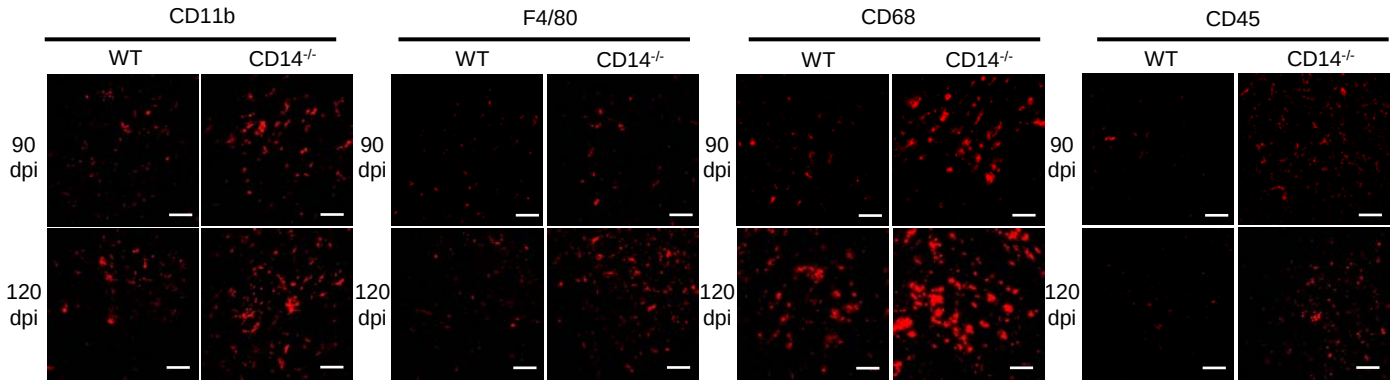

Fig. 7. Immunofluorescence staining for microglial markers in the brains of prion-infected WT and CD14$^{-/-}$ mice. Frozen blocks of the brains harvested at 90 and 120 dpi were subjected to immunofluorescence staining for microglial markers CD11b, F4/80, CD68, and CD45. Representative images from the thalamus of Chandler-infected mice are shown. Bars show 50 μm.

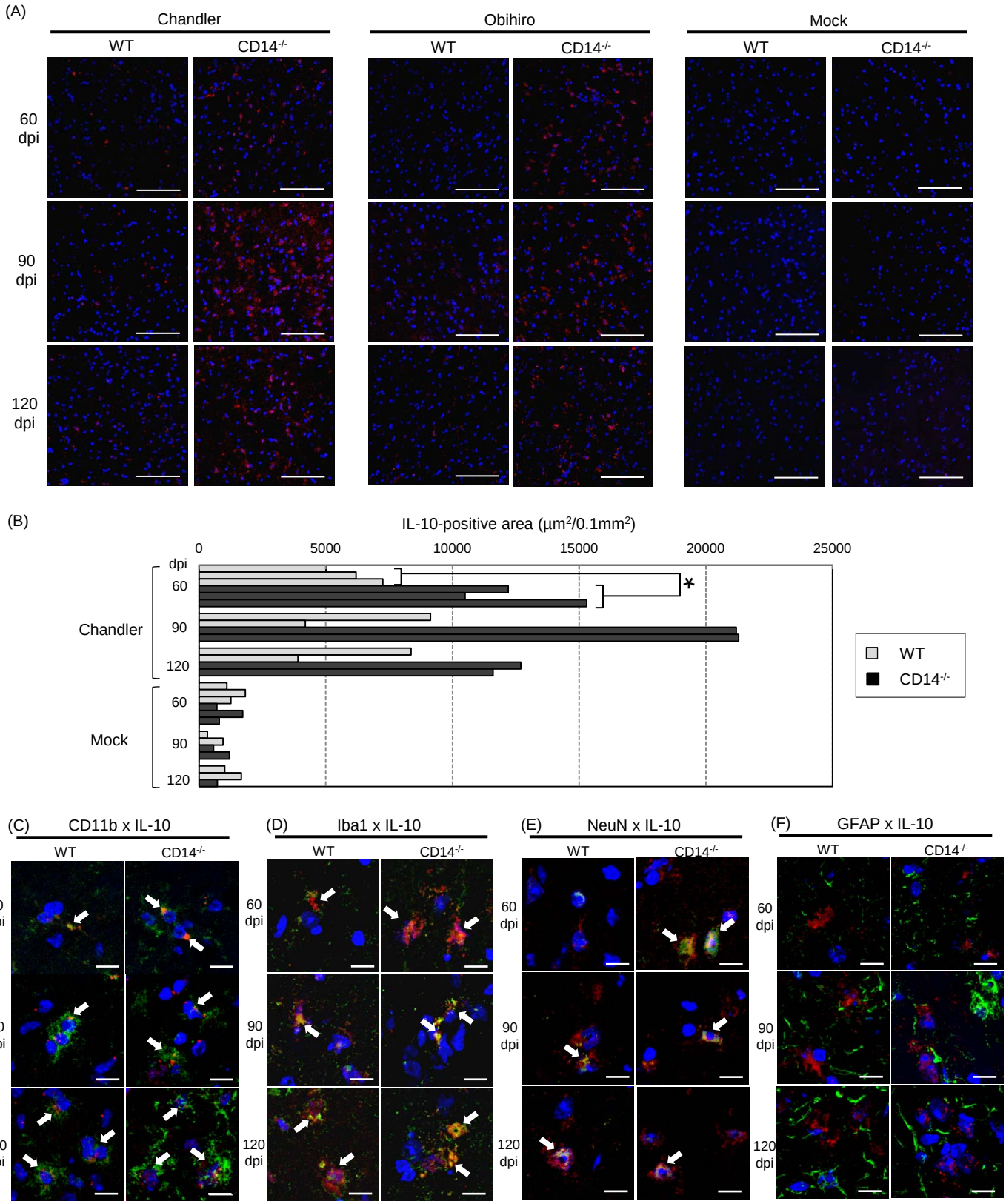

Fig. 8. Expression of IL-10 in the brains of WT and CD14$^{-/-}$ mice infected with the Chandler and Obihiro strains. (A) Immunofluorescence staining of IL-10. Frozen blocks of the brains harvested at 60, 90 and 120 dpi were subjected to immunohistochemistry. Representative figures from the thalamus at each time point were shown. Bars show 50 μm. Red, IL-10. Blue, DAPI. (B) Quantitative analysis of IL-10-positive areas in the thalamus of Chandler-infected mice. The areas positive for IL-10 (μm^2/0.1mm^2) were quantified using Imaris ver 7.6.1 (Bitplane). The numbers of mice used for the analysis were 3 both of WT and CD14$^{-/-}$ mice at 60 dpi, 2 both of WT and CD 14$^{-/-}$ mice at 90 dpi and 2 of WT mice at 120 dpi, and 1 of CD14$^{-/-}$ mouse at 120 dpi. ∗ p<0.01, Student's t-test. (C) – (F) Double immunofluorescence staining of IL-10 with CD11b (C), Iba1 (D), NeuN (E) and GFAP (F). Representative figures from the thalamus of Chandler-infected mice are shown. Green, CD11b (C), Iba1 (D), NeuN (E) and GFAP (F). Red, IL-10 Blue, DAPI. Arrows show the double positive cells. Bars show 10 μm.

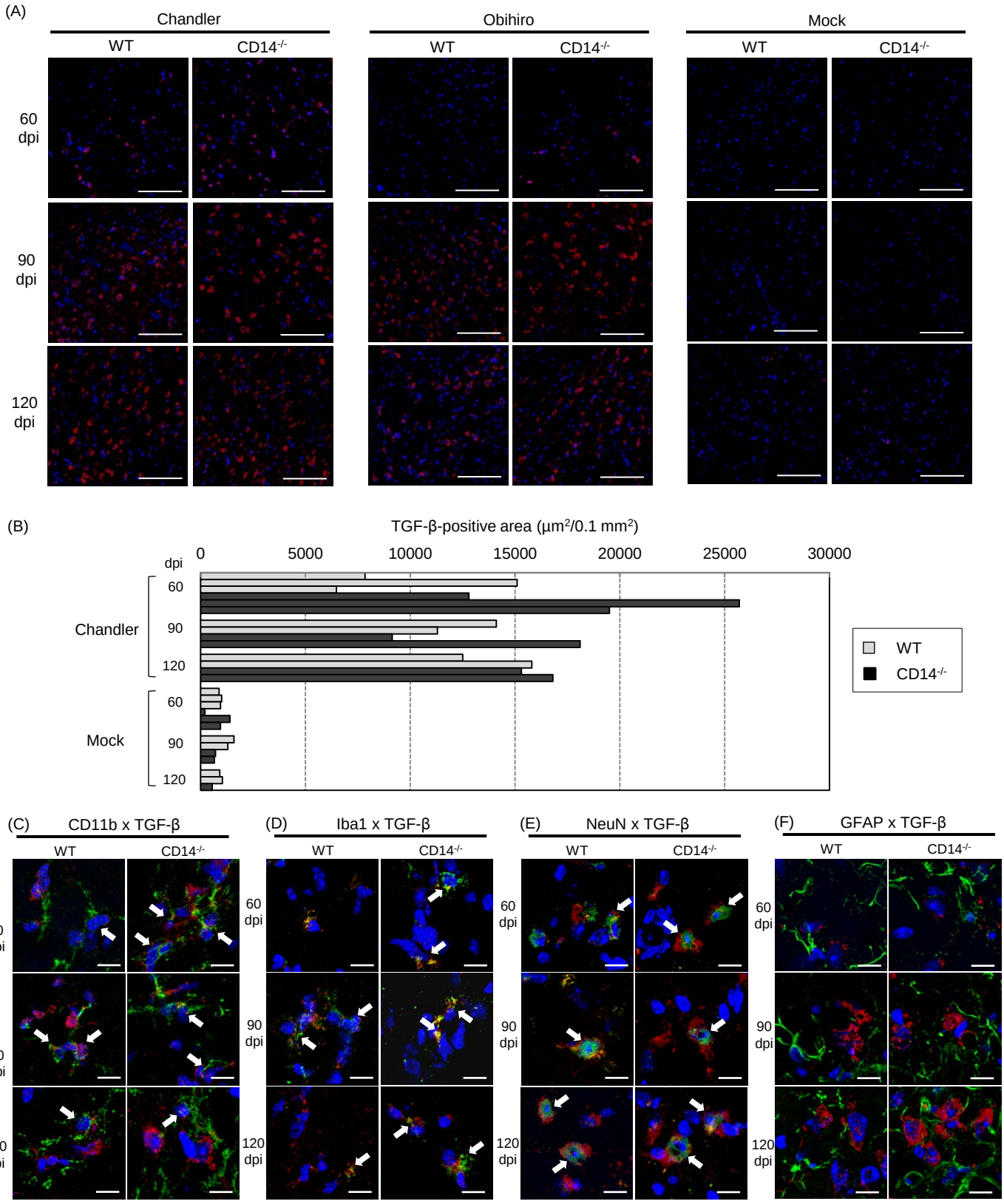

Fig. 9. Expression of TGF-β in the brains of WT and CD14$^{-/-}$ mice infected with the Chandler and Obihiro strains. (A) Immunofluorescence staining of TGF-β at 60, 90 and 120 dpi. Representative figures from the thalamus were shown for each time points. Bars show 50 μm. Red, TGF-β. Blue, DAPI. (B) Quantitative analysis of TGF-β-positive areas in the thalamus of Chandler-infected mice. The method and mice used for the quantification are the same as in the legend for Fig. 8. (C) – (F) Double immunofluorescence staining of TGF-β with CD11b (C), Iba1 (D), NeuN (E) and GFAP (F). Representative figures from the thalamus of Chandler-infected mice are shown. Green, CD11b (C), Iba1 (D), NeuN (E) and GFAP (F). Red, TGF-β. Blue, DAPI. Arrows show the double positive cells. Bars show 10 μm.

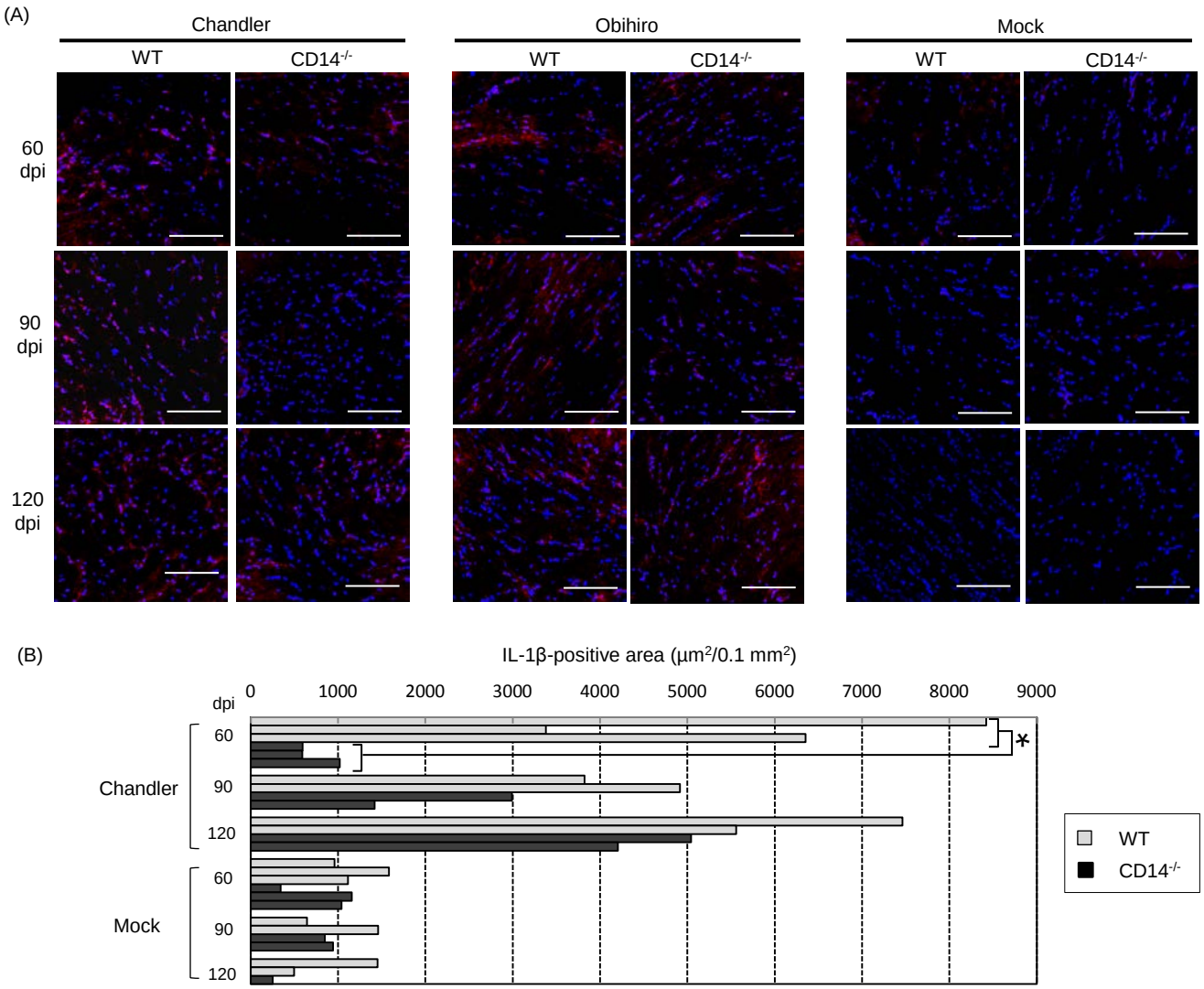

Fig. 10. Expression of IL-1β in the brains of prion-infected WT and CD14$^{-/-}$ mice. (A) Immunofluorescence staining of IL-1β in the internal capsule of mice infected with Chandler or Obihiro strains at 60, 90 and 120 dpi. Bars show 50 μm. Red, IL-1β. Blue, Nuclei. (B) Quantitative analysis of IL-1β-positive areas in the internal capsule of Chandler-infected mice. The method and mice used for the quantification are the same as in the legend for Fig. 8. * $p<0.05$, Welch *t*-test.